◆ Human Brain Mapping 33:2047–2061 (2012) ◆

Diffusion Tensor Imaging of the Optic Radiations After Optic Neuritis

Scott Kolbe,[1,2]* Clare Bajraszewski,[2] Caron Chapman,[2] Tan Nguyen,[3] Peter Mitchell,[4] Mark Paine,[3] Helmut Butzkueven,[1,2,5] Leigh Johnston,[1,6] Trevor Kilpatrick,[1,2,5] and Gary Egan[1,2]

[1]*Florey Neuroscience Institutes, Melbourne, Australia*
[2]*Centre for Neuroscience, University of Melbourne, Melbourne, Australia*
[3]*Neuro-Ophthalmology Unit, Royal Victorian Eye and Ear Hospital, Melbourne, Australia*
[4]*Department of Radiology, Royal Melbourne Hospital, Melbourne, Australia*
[5]*Department of Neurology, Royal Melbourne Hospital, Melbourne, Australia*
[6]*Department of Electrical and Electronic Engineering and the NICTA Victorian Research Laboratory, University of Melbourne, Melbourne, Australia*

Abstract: Trans-synaptic degeneration could exacerbate neurodegeneration in multiple sclerosis (MS). We aimed to assess whether anterograde trans-synaptic degeneration could be identified in the primary visual pathway in vivo. Diffusion tensor imaging (DTI) was used to assess the optic radiations in 15 patients with previous optic nerve inflammation and 9 healthy volunteers. A probabilistic atlas of the optic radiations was created from healthy diffusion tractography data. Lengthwise profiles for DTI parameters (axial [$\lambda_{||}$], radial [$\lambda_{\perp}$] and mean diffusivity [MD], fractional anisotropy [FA] and the angle of deviation of the principal eigenvector [α]) were analyzed for patients and controls. Patients also underwent multifocal visual evoked potential (mfVEP) assessments to characterize the latency and amplitude of cortical potentials. Correlations were performed between mfVEP latency and amplitude in the left and right visual hemi-fields and DTI parameters in the contra-lateral optic radiations. Patients displayed a significant decrease in $\lambda_{||}$ within the body of both optic radiations, which significantly correlated with loss of mfVEP amplitude. Abnormal $\lambda_{\perp}$ and FA were detected bilaterally throughout the optic radiations in patients but the abnormality was not associated with amplitude reduction or latency prolongation of the mfVEP. An abnormal α value was observed in the left optic radiations of patients, and the α value in the body of the optic radiations also correlated with mfVEP amplitude loss. The assocation between bilateral DTI abnormalities within the optic radiations and loss of afferent electrical activity could indicate anterograde trans-synaptic degeneration occurs following optic neuritis. *Hum Brain Mapp 33:2047–2061, 2012*.

Additional Supporting Information may be found in the online version of this article.

Contract grant sponsor: Australian National Health and Medical Research Council (NHMRC) Principal Research Fellowship, Australia; Contract grant number: 400317; Contract grant sponsor: Joint MS Research Australia/Trish MS Foundation/NHMRC Betty Cuthbert Fellowship; Contract grant number: 400476; Contract grant sponsors: The Joint MS Research Australia/Australian Financial Advisors Association Postgraduate Scholarship; Charityworks for MS, Melbourne; Neurosciences Victoria Neuro-Informatics Platform.

*Correspondence to: Scott Kolbe, Florey Neuroscience Institutes, University of Melbourne, Victoria, Australia.
E-mail: scott.kolbe@florey.edu.au

Received for publication 23 September 2010; Revised 27 February 2011; Accepted 11 April 2011

DOI: 10.1002/hbm.21343

Published online 13 September 2011 in Wiley Online Library (wileyonlinelibrary.com).

Key words: diffusion tensor imaging; multiple sclerosis; optic radiations

INTRODUCTION

Multiple sclerosis (MS) is characterized by multifocal inflammatory demyelinating lesions associated with significant axonal trans-section [Trapp et al., 1998]. However, in later stages of the disease, MS patients exhibit progressive brain atrophy [Chard et al., 2003] and neurological symptoms [Brex et al., 2002] in the relative absence of ongoing inflammatory activity. While the possibility exists that such progressive symptoms could result from inflammatory activity not observable using commonly employed magnetic resonance imaging (MRI) techniques, a more likely explanation is ongoing, secondary neurodegeneration, presumably initiated by early inflammatory activity.

One putative secondary neurodegenerative process is trans-synaptic neurodegeneration. Trans-synaptic degeneration has been shown to result from loss of synaptic inputs or neuronal signals from degenerating afferent neurons [Ghetti et al., 1972; Ginsberg and Martin, 2002; Glees et al., 1967; LeVay, 1971], or loss of neurotrophic factors from degenerating efferent neurons [Johnson and Cowey, 2000; van Buren, 1963]. Trans-synaptic degeneration can include altered synaptic, dendritic, and neuronal morphology and even neuronal apoptosis [Ghetti et al., 1972; LeVay, 1971]. In diseases characterized by focal brain injuries such as MS, trans-synaptic degeneration could elicit neurodegenerative processes in regions of the brain anatomically distant from the site of injury, thereby exacerbating neural dysfunction and clinical disability. However, the degree to which trans-synaptic degeneration contributes to neurodegeneration in patients with MS is unknown, as the phenomenon is difficult to characterize in vivo.

The primary visual pathway is potentially useful for studying trans-synaptic degeneration in the context of MS. The optic nerve is commonly affected by localized inflammatory demyelination, presenting as optic neuritis, which can lead to chronic demyelination and axonal degeneration within the optic nerve [Costello et al., 2006; Klistorner et al., 2007, 2008a; Kolbe et al., 2009; Trip et al., 2006b]. The altered synaptic input to the lateral geniculate nuclei (LGN) due to optic nerve demyelination and axonal degeneration is associated with neuronal injury within the LGN [Evangelou et al., 2001]. Therefore, assessments of optic nerve function using visual evoked potentials, and LGN injury using MRI, in patients with a history of optic neuritis could reveal anterograde trans-synaptic degeneration.

The LGN is small and difficult to define on T1-weighted structural MRI, rendering volumetric assessments of the nuclei challenging. However, the neuronal projections from the LGN to the visual cortex, which form the large collinear white matter tracts known as the optic radiations, can potentially be more easily assessed than the nuclei themselves. Diffusion weighted imaging (DWI), a MRI technique which is sensitive to the microscopic motion of water molecules in tissue, can sensitively reveal disruption to axonal and myelin microstructure in lesions and T2 normal-appearing white matter (NAWM) in MS [Rovaris and Filippi, 2007; Rovaris et al., 2005]. When diffusion is measured in six or more non-collinear directions, DWI data can be modeled using a tensor ellipsoid defined by three orthogonal eigenvectors (V_1, V_2, V_3) and three corresponding eigenvalues ($\lambda_1 > \lambda_2 > \lambda_3$) [Basser et al., 1994]. In white matter, the multitudinous microscopic parallel barriers produced by myelinated axons result in an anisotropic diffusion tensor ($\lambda_1 \gg \lambda_2 > \lambda_3$) with the principal eigenvector oriented axial to the direction of the fibre tract. Recent data from animal models of white matter injury have shown that restricted axial diffusivity ($\lambda_{||} = \lambda_1$) could be a marker for degenerating axons [DeBoy et al., 2007; Mac Donald et al., 2007a,b; Song et al., 2003; Wu et al., 2007; Zhang et al., 2009]. Conversely, increased radial diffusivity ($\lambda_\perp = [\lambda_2 + \lambda_3]/2$) has been observed in the presence of multiple white matter pathologies including demyelination [Song et al., 2003, 2005; Wu et al., 2008; Zhang et al., 2009], oedema and/or gliosis [Mac Donald et al., 2007a]. Consequently, white matter injury within the optic radiations could be a useful in vivo marker for anterograde trans-synaptic degeneration of LGN neurons.

While the optimal study design for characterizing trans-synaptic degeneration in the visual pathway would be a serial assessment of the radiations following acute optic neuritis, such a study will be expensive and require preliminary data to demonstrate feasibility. In contrast to a longitudinal study design, a cross-sectional design, while limited in interpretability regarding the timing of trans-synaptic degeneration, is significantly cheaper and can be used to assess effect sizes for power calculations for a subsequent longitudinal study. In addition, cross-sectional correlations can be used to infer relationships between optic radiation structure and optic nerve function. The aim of this study was therefore to assess DTI parameters ($\lambda_{||}$,$\lambda_\perp$, mean diffusivity [MD], fractional anisotropy [FA], and the angle of deviation of V_1 [α]) from T2 NAWM in 15 patients who presented with unilateral optic neuritis 4-years ago. We also assessed optic nerve axonal degeneration and demyelination using multifocal visual evoked potentials (mfVEP) [Klistorner et al., 2008b; Kolbe et al., 2009]. Use of multifocal stimulation allowed us to probe the function of the visual hemifields producing afferent visual inputs to the left and right optic radiations separately.

We aimed to characterize any observable DTI alterations in the optic radiations of these patients and assess correlative relationships between optic radiation DTI parameters and optic nerve dysfunction assessed using mfVEP, the

TABLE I. Summary demographic and disease data for patients

Patient characteristics	Mean	SD	Range	Ratio
Age (yrs)	34.8	7.7	22.6–49.7	—
Sex (F : M)	—	—	—	12 : 3
Time since acute optic neuritis (yrs)	4	0.4	3.4–4.8	—
Affected logMAR visual acuity	0.07	0.39	−0.3 to +1.0	11 left : 4 right
Unaffected logMAR visual acuity	−0.13	0.13	−0.3 to +0.18	—
T2 lesion volume (% BPV)	0.24	0.32	0–1.26	
Fulfillment of McDonald criteria for dissemination in space (Yes : No)	—	—	—	10 : 5

Abbreviations: yrs (years), F (female), M (male), BPV (brain parenchymal volume), CIS, (clinically isolated syndrome), SD (standard deviation of the mean).

identification of which could be used to inform the design of a prospective study.

SUBJECTS AND METHODS

Subjects

Fifteen patients (demographic and disease data are summarized in Table I), who presented with unilateral optic neuritis as a first demyelinating event 4.0 (± 0.4) years ago, were recruited to the study. All patients' clinical MRI scans were assessed by a neuroradiologist (PJM) at the time of imaging, and 10 patients satisfied the McDonald criteria for dissemination in space [McDonald et al., 2001]. MRI data from nine control subjects (7f/2m, mean ± SD age = 35.0 ± 10.7 years) with no reported history of neurological symptoms were used for statistical comparisons of DTI indices. MRI data from a further 11 control subjects (all male, mean ± SD age = 35.8 ± 12.6 years) were included in the calculation of the optic radiation atlas. Ethics approval for this study was granted by the Royal Melbourne Hospital Research Ethics Committee, and all subjects provided voluntary written consent to participate.

Brain MRI Acquisitions

All subjects were imaged using a Siemens 3 Tesla Trio TIM MRI system with a 12 channel receiver head coil (Siemens, Erlangen, Germany). All subjects were imaged using a high angular resolution diffusion weighted imaging sequence with the following parameters: matrix size = 128 × 128, FOV = 240 × 240 mm^2, 40 contiguous 3-mm thick axial slices providing whole brain coverage, gradient b-value = 1,000 s mm^{-2}, and GRAPPA parallel reconstruction with speed factor 2. DWI acquisition parameters varied slightly between some subjects as a result of a scanner operating system upgrade during the study. Twelve patients and six controls were scanned with the following parameters: five non-diffusion weighted images and 54 diffusion weighted images; TR = 5,800 ms; TE = 112 ms; while three patients and two controls were scanned using the parameters: five non-diffusion weighted images and 64 diffusion directions; TR = 4,400 ms; TE = 85 ms; and 11 controls were scanned with the parameters: 60 diffusion directions; TR = 5,000 ms; TE = 89 ms. Diffusion encoding gradients were applied according to an electrostatic repulsion algorithm [Jones et al. 1999].

In addition, patients underwent imaging using a 3D T2-weighted fluid-attenuated inversion recovery (FLAIR) sequence to identify T2 lesions in the optic radiations (TR = 6,000 ms, TE = 403 ms, TI = 2,100 ms, flip angle = 120°, ETL = 123, slice thickness = 1 mm, coverage = 176 mm, FOV = 256 × 222 mm^2, matrix size = 256 × 222). Lesions were defined on each patient's FLAIR image using a semi-automated local thresholding technique [Rorden and Brett, 2000] by a trained observer (SCK). All lesion masks were subsequently validated by a neuroradiologist (PJM). The lesion masks were linearly transformed to diffusion space using an affine registration algorithm [Jenkinson and Smith, 2001] and used to parcellate DTI maps into lesion and NAWM. Only NAWM was used in subsequent analyses.

Optic Radiation Mapping

White matter pathways such as the optic radiations can be anatomically identified using DWI data processed using tractography algorithms which serially sample the estimated principal direction of diffusion to produce streamlines of probable fibre pathways from a given seed region. However, the reduction in diffusion anisotropy caused by white matter injury can introduce noise into estimates of the principal direction of diffusion which in turn can cause spurious termination or divagation of tracts. Recent studies have attempted to address this problem through the use of probabilistic tract maps, which consist of tractography results calculated from multiple healthy subjects, normalized to a standard brain space [Hua et al., 2008; Lin et al., 2007; Pagani et al., 2005; Reich et al., 2009b]. The standard space tract maps can be registered to patient quantitative MR images to obtain tract-specific measurements.

A probabilistic atlas of the optic radiations was generated using control DWI data from 20 healthy subjects (7f/13m, mean ± SD age = 35.4 ± 11.8 years). This group included the 9 control subjects described above used for case-control comparisons together with data from an additional 11 healthy subjects obtained from a local imaging database. The additional subjects were included to improve the anatomical accuracy of the probability map. Imaging parameters for data from the imaging database were as follows: 60 diffusion directions; TR = 5,000 ms; TE = 89 ms; matrix size = 128 × 128, FOV = 240 × 240 mm^2, 40 contiguous 3-mm thick axial slices providing whole brain coverage, gradient *b*-value = 1,000 s mm^{-2}, and GRAPPA parallel reconstruction with speed factor 2.

The analytical procedures used to generate the optic radiation probability map are summarized in Figure 1. Raw diffusion weighted images were eddy-current and motion corrected by affine registration of all the images to the first non-diffusion weighted image using a linear registration algorithm (FLIRT) [Jenkinson and Smith, 2001]. The diffusion tensor and associated $\lambda_{||}$, $\lambda_{\perp}$, MD, FA, and V_1 maps were calculated for each subject using FSL [Smith et al., 2004]. For each subject, the FA map was aligned with a standard space FA template [Mori et al., 2008] using FLIRT, followed by a non-linear deformation (FNIRT, FSL, Oxford) (Fig. 1A). The resulting deformation fields were used in all subsequent transformations to standard space and inverse deformation fields were used to transform images from standard space back to each subject's acquired image space. Vector fields for V_1 were non-linearly transformed using the deformation fields and the preservation of principal direction (PPD) algorithm [Alexander et al., 2001].

Diffusion tractography was subsequently used to define the optic radiations in control subjects. Seed, waypoint and termination masks (Fig. 1B) were defined in standard space. The seed masks (LGN) and secondary waypoint masks (primary visual cortex) were obtained from a probabilistic histological atlas [Eickhoff et al., 2005]. Waypoint masks in the anterior optic radiations were drawn on the template image according to a published protocol [Xie et al., 2007]. All masks were transformed to each control subject's acquired image space. Tractography was performed using the FSL diffusion toolkit (www.fmrib.ox.ac.uk/fsl). The FSL diffusion toolkit uses a local diffusion model (BEDPOSTX) which estimates a probability distribution for the PDD in each voxel accounting for the possibility of more than one fibre direction [Behrens et al., 2007]. Tractography was then performed using a probabilistic streamline algorithm (PROBTRACKX) which generates streamlines by serially sampling the PDD distributions [Behrens et al., 2007]. Probabilistic streamlines were calculated for tracts from the left and right LGN. Only streamlines which passed through both waypoint masks in the anterior optic radiation and primary visual cortex and did not cross the termination mask were considered valid optic radiation streamlines. The resulting "connectivity" images contained values which represent the number of probabilistic streamlines which passed through each voxel. Voxels which had values less than 10% of the total streamlines which passed through the waypoints were excluded from the tract images (10% was an arbitrary conservative value applied consistently to remove voxels with low probability of being included in the tract). The thresholded tracts were then binarised to create binary tract masks.

The binary tract masks were normalized to standard space and the final optic radiation probability map was calculated by averaging the binary tract masks at each voxel for the control group to produce probability values between 0 (tract in no subjects) and 1 (tract in all subjects) (Fig. 1C). The probability map was then transformed to each patient and control subject's acquired image space. In patients, voxels classified as lesion based on FLAIR hyperintensity were excluded from the probability map. In controls and patients, any remaining probability map voxels where MD $>2.1 \times 10^{-3}$ mm^2 s^{-1} (CSF) or FA < 0.2 (gray matter) were excluded.

Optic Radiation Probability Map Reliability Assessments

The reliability of the probability map was assessed in two ways. The first method, similar to that used by Pagani et al. [2005], was to determine whether there were systematic differences in $\lambda_{||}$, $\lambda_{\perp}$, MD, and FA calculated from independently generated probability maps. Control subjects were randomly assigned to two groups (denoted "group A" and "group B"). Two independent optic radiation probability maps were calculated using data from each group. The two maps were used to calculate weighted mean values for $\lambda_{||}$, $\lambda_{\perp}$, MD, and FA for each control subject and patient. Limits of agreement (the 95% confidence interval for the differences between two measurements made using two methods) were calculated for DTI parameters obtained using the two maps using the method proposed by Altman and Bland [1983]. Limits of agreement for DTI parameters calculated from the two independently generated probability maps were less than 2% of the mean of the measurements for all DTI parameters calculated from controls ($\lambda_{||}$: 1.47%; $\lambda_{\perp}$: 1.57%; MD: 0.77%; FA: 0.88%) and patients ($\lambda_{||}$: 0.78%; $\lambda_{\perp}$: 1.51%; MD: 1.85%; FA: 1.27; Supporting Information Fig. 1A).

The second method, similar to that used by Hua et al. [2008], was to determine the agreement between $\lambda_{||}$, $\lambda_{\perp}$, MD, and FA calculated using the probability map and corresponding DTI parameters calculated from ROIs based on thresholded individual tractography results in control subjects. The individual tractography maps for each control subject were thresholded to exclude voxels with FA < 0.2, binarized, and multiplied by the $\lambda_{||}$, $\lambda_{\perp}$, MD, and FA maps. Limits of agreement were calculated for $\lambda_{||}$, $\lambda_{\perp}$, MD, and FA for probability map data and individual tractography ROI data. Limits of agreement were between five

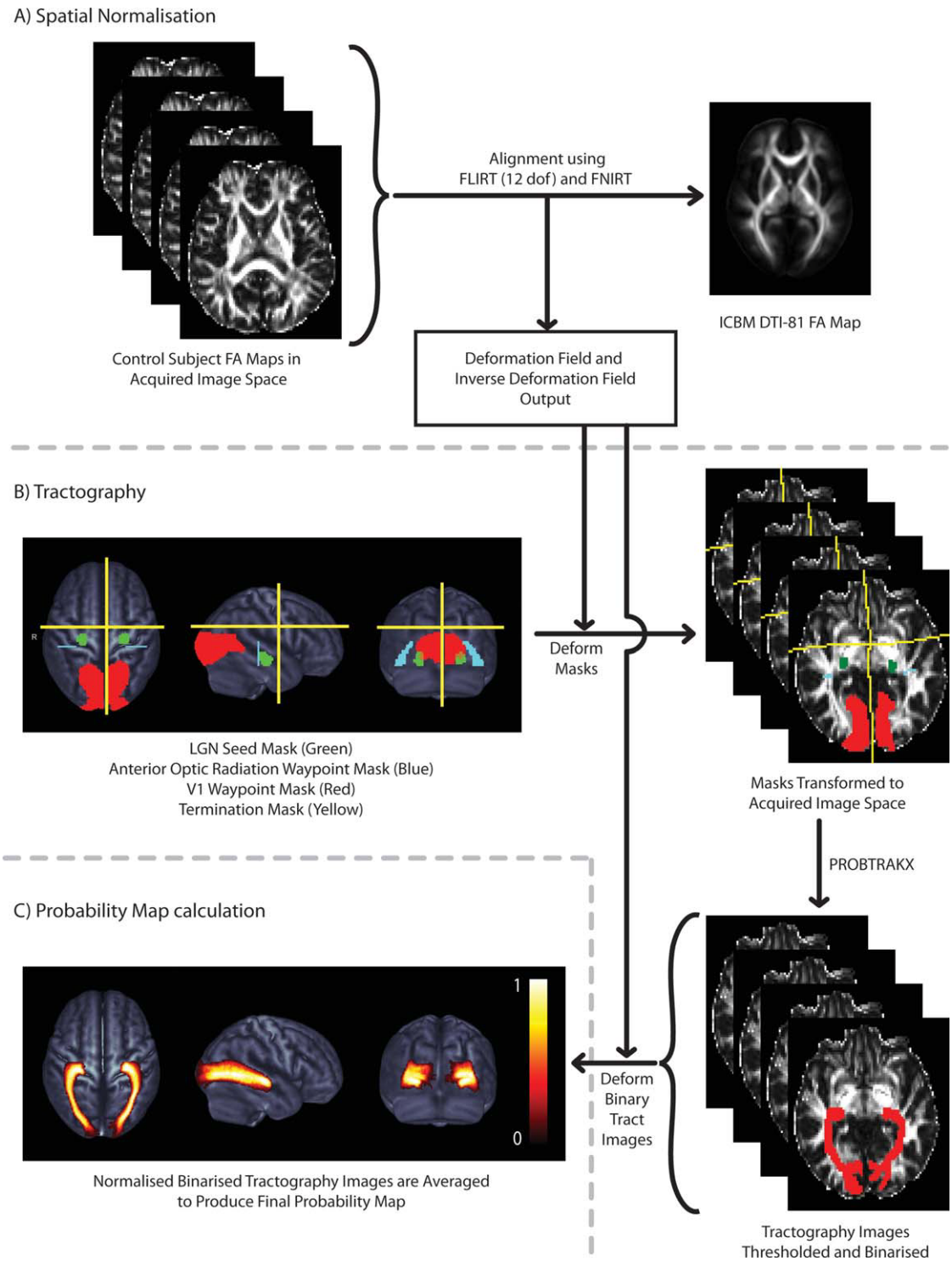

Figure 1.

Illustrates the methodology used to create the probability map of the optic radiations. (**A**) Each subject's FA image was registered to the ICBM template FA image using a two-step registration procedure involving an initial linear alignment followed by a nonlinear deformation. The deformation field and inverse deformation field were output. (**B**) Seed masks in the lateral geniculate nuclei (LGN, green), waypoint masks in the anterior optic radiation (blue) and primary visual cortex (V1, red) and termination masks used to remove spurious interhemispheric, anterior and superior projecting streamlines (yellow) were defined in standard space, deformed to each subject's DW image space and used for probabilistic tractography. (**C**) Individual subject binary tract images were deformed to standard space and averaged to created the probability map which is displayed here as an orthogonal maximum intensity projection. [Color figure can be viewed in the online issue, which is available at wileyonlinelibrary.com.]

and 13% of the mean of the two measurements ($\lambda_{||}$: 5.68%; $\lambda_{\perp}$: 12.97%; MD: 7.33%; FA: 13.17%; Supporting Information Fig. 1B).

These reliability assessments demonstrated that the probability mapping method produced robust DTI parameters in both controls and patients independent of the subjects used to calculate the map. However, there was poorer agreement between DTI parameters calculated using probability maps and those calculated using individual tractography data.

Optic Radiation DTI Parameter Assessments in Patients and Controls

Average $\lambda_{||}$, $\lambda_{\perp}$, MD, and FA were calculated for controls and patient NAWM, weighted according to the optic radiation probability map. In addition, the probability maps were parcellated into 40 cross-sections, from the LGN to V1, to study potential localized patterns of DTI abnormalities in patients. The procedure for defining the cross-sections was developed in MATLAB7 (www.mathworks.com). First the tract centreline was defined for left and right optic radiations as the voxel with maximum probability in each coronal slice. Second, at each centre point, a circle of radius 10 mm was defined orthogonal to the vector joining the centres of the proximal and distal centre point voxel neighbours. The intersection of this circle with probability map voxels was defined as a cross-section. Forty such cross-sections were defined for left and right optic radiations. Average DTI indices were calculated and weighted according to the optic radiation probability map, at each cross-section. For patients, only NAWM voxels were included.

Recent evidence has suggested that white matter injury could result in incorrect estimation of V_1, thus also rendering inferential assessments of "axial" and "radial" diffusivities inaccurate [Wheeler-Kingshott and Cercignani, 2009]. We therefore quantitatively assessed angular deviation in the direction of V_1 in patients and controls. To do this we first calculated, in standard space, a reference map for V_1 (V_1^{ref}) by averaging cartesian elements (x, y, z) of the normalized V_1 vectors for the healthy volunteer group. The average cartesian vectors were then voxelwise length normalized. We then performed voxelwise calculations of the absolute angle of deviation (α) of V_1 in each subject (V_1^{subj}) from V_1^{ref} using the arc-cosine of the dot product of the reference vector to the subject's vector:

$$\alpha = \arccos(V_1^{\mathrm{ref}} \cdot V_1^{\mathrm{subj}})$$

Scalar maps of α for each control and patient were converted from radians to degrees and analyzed using the same procedures used for maps of $\lambda_{||}$, $\lambda_{\perp}$, MD, and FA. An example of image for a control subject in standard space is available as Supporting Information (Supporting Information Fig. 2). All calculations on V_1 were performed using MATLAB7.

Multifocal VEP

Multifocal VEP data was acquired using Accumap mfVEP system (ObjectiVision, Sydney, Australia) by a trained technician. Patients viewed a computer screen where a dartboard configuration was used to display reversing black and white checks in pseudo-random binary sequences. Fifty-eight such checks were used to stimulate sectors spanning the central 24° of the visual field. Four gold electrodes placed around the inion recorded 10–12 runs of 55 s stimulation for each eye. The signal corresponding to each visual field sector was subsequently calculated using cross-correlation of the response with the stimulus sequence. The average peak-to-trough amplitude and latency of the VEP was calculated for VEP waveforms in each visual field sector and averaged across each visual hemifield.

To characterize visual dysfunction associated with optic nerve injury in the clinically affected side while removing functional variability associated with the unaffected side we calculated the interocular percentage difference for amplitude and latency for each hemifield.

Statistical Analyses

Group differences in DTI parameter profiles obtained from control and patient left and right optic radiations were compared using two-way repeated measures analyses of variance (repeated measures: segment; fixed factors: group, sequence). Main effects for group and DWI sequence as well as the interactions group × segment, group × sequence, and group × segment × sequence were tested for significance. In the case that the modeled interaction group × segment was significant indicating a regional DTI abnormality, post-hoc t tests were performed between control and patient DTI parameters for each segment to identify the anatomical location of the regional abnormality.

Correlation analyses between left and right optic radiation DTI parameters and left and right hemifield visual asymmetry were performed using Pearson's parametric correlation coefficients.

All statistical analyses were performed using PASW Statistics 18.0 for Mac (SPSS, Chicago, USA). To account for multiple statistical tests, only $P < 0.01$ was considered significant with $P < 0.05$ reported as a non-significant trend.

RESULTS

Optic Radiation DTI Profiles in Controls

The geniculo-striate profiles for DTI parameters from control optic radiations were similar between left and right hemispheres (see Fig. 2). The LGN (Segments 1–3) showed increasing $\lambda_{||}$ and FA consistent with the interfacing of grey and white matter. Segments 4–10, corresponding with

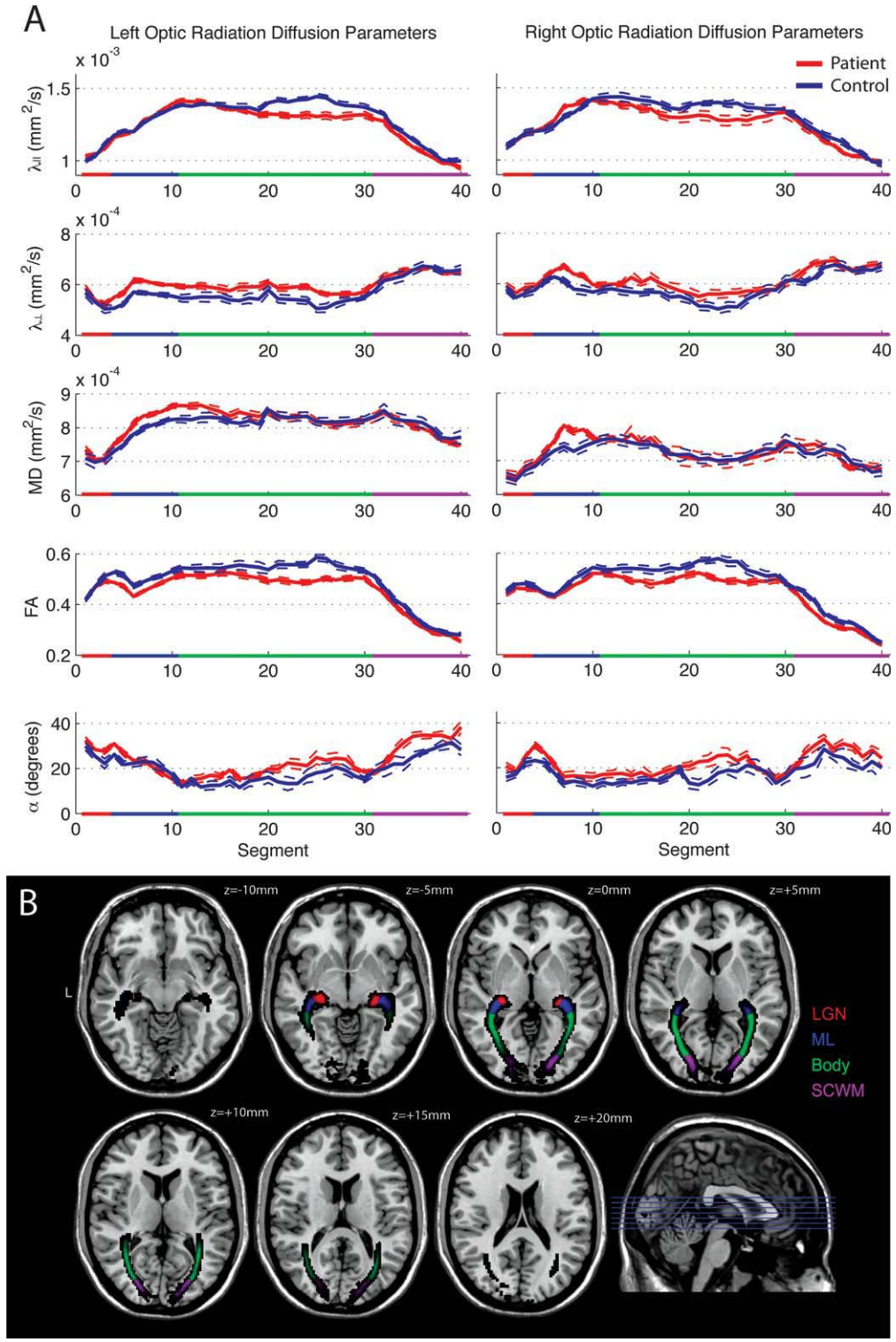

Figure 2.

(**A**) Mean DTI parameter profiles for the left and right optic radiation NAWM, measured from 40 segments from LGN (0) to cortex (40). Dashed lines indicate standard error of the mean. Anatomical subregions of the optic radiations are color coded as follows: lateral geniculate nuclei (LGN, red), Meyer's loop (ML, blue), the body of the optic radiations (Body, green), and the subcalcarine white matter (SCWM, purple). (**B**) Axial slices of the probability map in MNI space colour coded to illustrate the anatomical distribution of the optic radiation subregions. [Color figure can be viewed in the online issue, which is available at wileyonlinelibrary.com.]

the location of Meyer's loop in the ventral optic radiations, displayed a trough in FA, which was associated with a peak in $\lambda_{\perp}$ and α. These DTI changes are consistent with a high rate of angular change in V_1 within the loop. Distal to Meyer's loop (Segments 11–30) the body of the optic radiations displayed high $\lambda_{||}$ and FA and relatively low $\lambda_{\perp}$ and α, indicative of tightly packed, collinear axon bundles. However, in distal regions of the radiations (Segments 31–40), FA progressively decreased, associated with a progressive decrease in $\lambda_{||}$ and an increase in $\lambda_{\perp}$. The reduction in anisotropy near the cortex was potentially associated with the intersection of the geniculostriate fibres by orthogonal intra-cortical fibres connecting primary and higher visual cortices. The parcellation of the optic radiations based on these DTI patterns (LGN, Meyer's loop, body and subcalcarine white matter) corresponds to a published microsurgical parcellation [Peltier et al., 2006].

Optic Radiation DTI Alterations after Optic Neuritis

Optic radiation lesions were observed in the left optic radiations in 12 patients (mean ± SD volume of tract = 2.1% ± 2.7%; range = 0–8.1%) and in the right optic radiations in 14 patients (mean ± SD volume of tract = 4.3% ± 3.7%; range = 0–13.0%). The right optic radiation of a single patient contained 28.4% lesional volume, and that optic radiation was excluded from subsequent analyses to minimize the potential effects of peri-lesional white matter injury on NAWM DTI measures.

Two DWI sequences were used to acquire control and patient data. Therefore we included "sequence" as a factor in our analyses of variance to investigate the influence of MR sequence on DTI parameter comparisons. A significant main effect for "sequence" was observed for $\lambda_{\perp}$ and FA (Table II). However, no significant interaction was observed between "group" and "sequence" for either $\lambda_{\perp}$ or FA, indicating that alterations in these measures due to sequence variation did not influence group differences. No significant three-way interaction between "group," "segment," and "sequence" was observed for any DTI parameter, indicating that differences in DWI sequences did not affect sensitivity to regional abnormalities in DTI parameters.

Analyses of variance revealed a significant main effect for "group" for $\lambda_{\perp}$ bilaterally, FA bilaterally and α within the left optic radiation (Table III). A significant interaction between "group" and "segment" was observed for $\lambda_{||}$ bilaterally and FA bilaterally. Multiple segment-wise unpaired t tests confirmed that regional abnormality ($P < 0.01$) in $\lambda_{||}$ was located within the body of the optic radiations bilaterally (left: Segments 20–27; right: Segments 22–25) and regional abnormality in FA was located in the left Meyer's Loop (Segments 4–8) and the body of the optic radiations bilaterally (left: Segments 21–28; right: Segments 22–25).

TABLE II. F statistics and *P*-values for the main effects and interactions of "sequence" tested using repeated-measures ANOVA

		F statistic (significance)	
Dependant variable	Explanatory model	Left optic radiation	Right optic radiation
$\lambda_{||}$	Sequence	0.15	0.51
	Sequence × Group	0.81	0.18
	Sequence × Group × Segment	0.89	1.17
$\lambda_{\perp}$	Sequence	9.62 ($P = 0.006$)	9.54 ($P = 0.006$)
	Sequence × Group	0.49	1.24
	Sequence × Group × Segment	0.5	1.18
MD	Sequence	0.72	4.29
	Sequence × Group	0.05	0.14
	Sequence × Group × Segment	0.6	1.22
FA	Sequence	15.30 ($P = 0.001$)	8.46 ($P = 0.009$)
	Sequence × Group	1.85	4.65 ($P = 0.04$)
	Sequence × Group × Segment	0.65	0.83
α	Sequence	0.02	0.02
	Sequence × Group	0.7	0.03
	Sequence × Group × Segment	0.5	0.91

These results confirm that despite the existence of a main effect for sequence for radial diffusivity and fractional anisotropy, no interaction terms were significant indicating that differences in DTI parameters attributable to DWI sequence did not affect group comparisons

Abbreviations: $\lambda_{||}$ (axial diffusion coefficient), $\lambda_{\perp}$ (radial diffusion coefficient), MD (mean diffusivity), FA (fractional anisotropy), α (angle of deviation of the principal eigenvector).

Optic Nerve Dysfunction in Patients

Visual evoked potential trace waveforms recorded from patients' clinically affected eyes displayed significantly reduced amplitude for the left (affected mean ± SD = 0.149 ± 0.048 μV; unaffected mean ± SD = 0.221 ± 0.062 μV; $P < 0.0001$) and right (affected mean ± SD = 0.167 ± 0.054 μV; unaffected mean ± SD = 0.236 ± 0.080 μV; $P = 0.002$) visual fields compared to unaffected eyes. Latency was significantly increased for the right (affected mean ± SD = 149.8 ± 10.2 ms; unaffected mean ± SD = 143.0 ± 8.4 ms; $P < 0.0001$) but not the left (affected mean ± SD = 144.8 ± 10.8 ms; unaffected mean ± SD = 145.2 ± 8.8 ms; $P = 0.88$) visual fields in affected compared to unaffected eyes.

TABLE III. *F* statistics and *P*-values for the main effects and interactions of "group" and "segment" for left and right optic radiations tested using repeated-measures ANOVA

		F statistic (significance)	
Dependant variable	Explanatory model	Left optic radiation	Right optic radiation
$\lambda_{\|\|}$	Group	3.55	2.44
	Group × Segment	5.33 ($P < 0.0001$)	2.93 ($P < 0.0001$)
$\lambda_{\perp}$	Group	13.78 ($P = 0.001$)	9.01 ($P = 0.007$)
	Group × Segment	0.91	1.12
MD	Group	0.9	0.62
	Group × Segment	1.58 ($p = 0.02$)	1.59 ($P = 0.02$)
FA	Group	25.13 ($P < 0.0001$)	31.64 ($P < 0.0001$)
	Group × Segment	1.83 ($P = 0.002$)	1.68 ($P = 0.006$)
α	Group	10.85 ($P = 0.004$)	7.23 ($P = 0.02$)
	Group × Segment	0.92	0.72

Abbreviations: $\lambda_{\|\|}$ (axial diffusion coefficient), $\lambda_{\perp}$ (radial diffusion coefficient), MD (mean diffusivity), FA (fractional anisotropy), α (angle of deviation of the principal eigenvector).

Optic Radiation Injury Correlates With Optic Nerve Injury

Our central hypothesis was that injury to the optic nerve following optic neuritis could lead to injury to second order neurons in the LGN, resulting in abnormalities in their axonal projections into the optic radiations. After confirming significant DTI abnormalities in the optic radiations, we wanted to test whether these were associated with loss of functional input to the LGN measured as mfVEP amplitude loss and mfVEP latency prolongation. As all patients presented with unilateral lesions with no subsequent contra-lateral attacks of optic neuritis, we calculated percentage asymmetries for mfVEP amplitude and latency in order to capture only dysfunction associated with optic neuritis. Asymmetries for the left and right visual hemifields were correlated with DTI parameters measured from subregions (LGN, Meyer's Loop, body, subcortical white matter) of the contra-lateral optic radiation (Table IV, Fig. 3A).

Reduced $\lambda_{\|\|}$ ($R = -0.450$, $P = 0.009$) and increased α ($R = 0.479$, $P = 0.008$) in the body of the optic radiations were both associated with greater asymmetry in mfVEP amplitude (Fig. 3B). To determine whether $\lambda_{\|\|}$ and α were collinearly related to mfVEP amplitude asymmetry, we performed a post-hoc multiple regression analysis including mfVEP amplitude asymmetry as the dependent and $\lambda_{\|\|}$ and α as competing independent variables. The model including both variables was significant ($R = 0.585$, $P = 0.004$) with both independent variables showing a strong trend towards independent contributions ($\lambda_{\|\|}$: $\beta_{std} = -0.348$, $P = 0.04$; α: $\beta_{std} = 0.388$, $P = 0.03$).

DISCUSSION

Trans-synaptic degeneration could cause significant and widespread secondary neurodegeneration in MS, but is difficult to assess in vivo. Histological evidence supports a role for anterograde trans-synaptic degeneration in the primary visual pathway, given that optic nerve axonal degeneration is associated with LGN neuron loss in MS autopsy cases [Evangelou et al., 2001]. The current study investigated chronic DTI alterations in the optic radiations four years after an episode of acute unilateral optic neuritis and assessed correlations between optic radiation DTI abnormalities and the degree of optic nerve dysfunction, assessed using mfVEP. In summary, we observed significant differences in axial and radial diffusivities, diffusion anisotropy and tensor directionality in the optic radiations between patients and controls. Significant correlations were detected between asymmetry in hemi-field VEP amplitude, potentially indicative of optic nerve axon loss, and contra-lateral optic radiation $\lambda_{\|\|}$ and α. In contrast, asymmetry in hemi-field VEP latency, potentially indicative of optic nerve demyelination, did not significantly correlate with any DTI parameters in the optic radiations. These results suggest that chronic loss of afferent electrical activity could injure second order neurons in MS.

DTI Alterations in Patients

We observed a reduction in $\lambda_{\|\|}$ regionally restricted to the body of the optic radiations. In contrast, $\lambda_{\perp}$ was increased throughout the length of the radiations. Reduced $\lambda_{\|\|}$ has previously been associated with acutely injured axons in animal models [DeBoy et al., 2007; Mac Donald et al., 2007a,b; Song et al., 2003; Wu et al., 2007; Zhang et al., 2009] and humans [Concha et al., 2006]. However, subsequent changes to the cellular milieu such as oedema, demyelination, and inflammation can all lead to a secondary increase in isotropic diffusion, accompanied by a recovery or increase in axial diffusivity compared to baseline [Mac Donald et al., 2007a]. Indeed, reduced $\lambda_{\|\|}$ has recently been reported in the optic nerves of human patients during acute optic neuritis [Naismith et al., 2009] but chronically, both $\lambda_{\|\|}$ and $\lambda_{\perp}$ have been shown to be elevated [Kolbe et al., 2009; Trip et al., 2006a]. The observed increase in $\lambda_{\perp}$ potentially reflects subtle diffuse white matter injuries which could include demyelination [Song et al., 2003, 2005] as well as oedema and gliosis [Mac Donald et al., 2007a]. The reduction in $\lambda_{\|\|}$ and accompanying increase in $\lambda_{\perp}$ resulted in no change in MD but a significant reduction in FA throughout the radiations.

TABLE IV. Coefficients (and *P*-values where significant) for Pearson correlation analyses between DTI parameters measured from left and right optic radiation subregions and contralateral hemifield mfVEP amplitude asymmetry, mfVEP latency asymmetry, and lesion volume within the whole optic radiation

Optic radiation DTI parameter	Correlate	Optic radiation subregion			
		LGN	ML	Body	SCWM
$\lambda_{\|\|}$	Amplitude asymmetry	−0.110	0.050	0.450 ($P = 0.009$)	−0.260
	Latency asymmetry	0.143	0.063	−0.310	0.012
	Lesion volume	−0.066	−0.010	−0.263	0.037
$\lambda_{\perp}$	Amplitude asymmetry	−0.235	−0.005	0.045	−0.007
	Latency asymmetry	−0.082	0.225	−0.083	0.137
	Lesion volume	−0.187	0.261	0.136	−0.027
MD	Amplitude asymmetry	−0.193	−0.027	−0.226	−0.124
	Latency asymmetry	0.012	0.171	−0.223	0.097
	Lesion volume	−0.140	0.159	−0.067	0.004
FA	Amplitude asymmetry	0.135	−0.033	−0.365 ($P = 0.05$)	−0.121
	Latency asymmetry	0.205	−0.158	−0.139	−0.025
	Lesion volume	0.197	−0.252	−0.360	0.079
α	Amplitude asymmetry	0.150	0.287	0.479 ($P = 0.008$)	0.125
	Latency asymmetry	−0.150	−0.260	0.057	0.087
	Lesion volume	−0.100	−0.075	−0.002	0.041

Abbreviations: $\lambda_{\|\|}$ (axial diffusion coefficient), $\lambda_{\perp}$ (radial diffusion coefficient), MD (mean diffusivity), FA (fractional anisotropy), α (angle of deviation of the principal eigenvector), LGN (lateral geniculate nuclei), ML (Meyer's Loop), SCWM (subcalcarine white matter).

When interpreting directional diffusivity abnormalities it is important to note that $\lambda_{\|\|}$ and $\lambda_{\perp}$ represent diffusivity measures which are parallel and perpendicular to the principal eigenvector, V_1, not the underlying axonal tract as is commonly assumed. A recent paper by Wheeler-Kingshott and Cercignani [2009] illustrated that alterations to the raw diffusion-weighted imaging signal due to white matter pathology can lead to alteration in the estimated direction of V_1, particularly in white matter characterised by non-collinear axonal fibres. In order to quantitatively compare the direction of V_1 between patient and control optic radiations, V_1 was normalized for each subject using the previously estimated deformation fields and the PPD algorithm used by Wheeler-Kingshott and Cercignani [2009]. From the normalized V_1 vectors, we calculated the angle of deviation, α, from the average control V_1. A significant increase in the α measure was observed in the left optic radiation of patients compared to controls, and a near-significant trend was observed in the right optic radiation. The cause of the change in $V1$ direction is difficult to interpret but potentially reflects disorganization or tortuosity of injured axonal fibres, as has been observed histologically in postmortem MS tissue [Craner et al., 2004]. Further studies investigating microstructural correlates of DTI in MS will be required to better understand the biological causes of alterations in V_1 direction in NAWM.

We observed significant correlations between reduction in $\lambda_{\|\|}$ and increase in α in the body of the optic radiations and loss of optic nerve signal transduction. Post-hoc multiple linear regression confirmed that both $\lambda_{\|\|}$ and α values showed a trend toward independent associations with mfVEP amplitude loss. Chronic loss of visual evoked potential amplitude is commonly believed to result from transection of optic nerve axons or retinal ganglion cell degeneration. Conversely, prolongation of VEP is commonly believed to reflect extant demyelination. We did not observe correlations between hemi-field mfVEP latency asymmetry and any optic radiation DTI parameter. These results suggest that optic nerve axonal degeneration and the resulting loss of afferent connections to the LGN following severe optic neuritis can induce changes in LGN neurons which in turn alter the direction and magnitude of the principal diffusion direction in the optic radiations.

Two alternative hypotheses for the observed optic radiation NAWM DTI alterations are (a) Wallerian or retrograde degeneration of axons due to inflammatory activity within the radiations themselves, or (b) retrograde degeneration due to cortical lesions within $V1$. No significant correlations were detected between optic radiation lesion volume and any NAWM DTI parameter in any subregion, rendering the first alternative hypothesis unlikely. A previous study [Reich et al., 2009c] also assessed correlations between optic radiation NAWM DTI parameters and those measured from lesions as indicators of lesion severity. We did not perform such an analysis because some optic radiations contained no lesions and therefore assessments of lesional DTI in those radiations were impossible. The possibility exists that cortical lesions could have contributed to the DTI alterations observed. Cortical lesions are difficult to observe using conventional image contrasts but have been successfully identified using double inversion recovery sequences [Geurts et al., 2005] which were not used in this study.

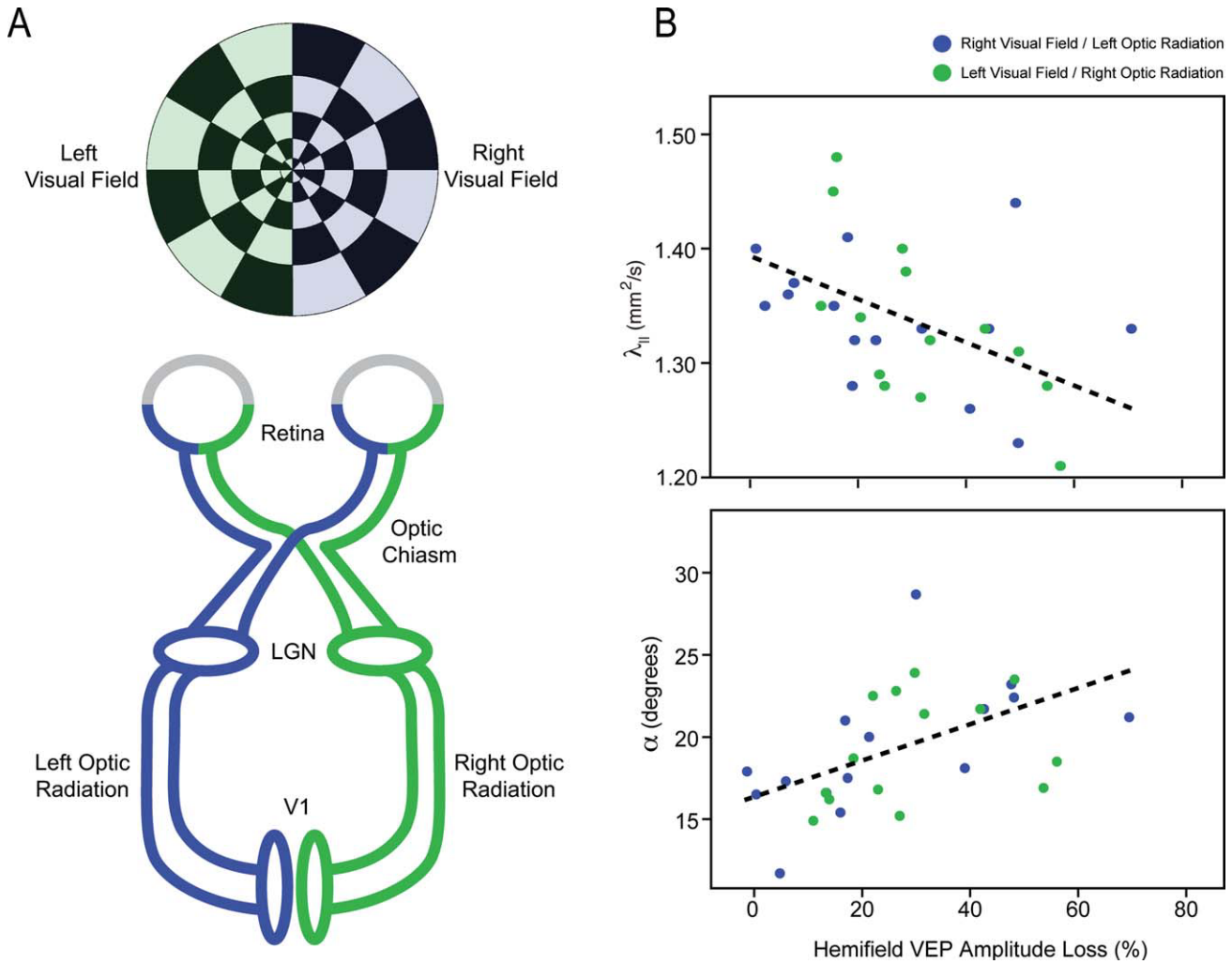

Figure 3.

(**A**) Schematic illustrating the connectivity of the primary visual pathway. Cortical activity induces by stimulation of the left (green) or right (blue) visual hemifields was assessed using mfVEP. Left (blue) and right (green) optic radiation injury was assessed using DTI. (**B**) Scatterplots illustrating the correlative relationships between $\lambda_{||}$ and α measured from the normal-appearing white matter of the body of the optic radiations in patients and mfVEP attenuation in the visual hemifield of clinically affected side. [Color figure can be viewed in the online issue, which is available at wileyonlinelibrary.com.]

Comparisons With Previous Post-Geniculate Imaging Studies of Patients With Optic Nerve Injury

A previous optic radiation diffusion MRI study of the optic radiations by Ciccarelli et al. [2005] reported a no significant differences in FA in the optic radiations of patients with extant optic neuritis of 1 year, compared to controls. The authors did, however, detect significant differences in the location of the tracts and in the probabilistic connectivity values obtained from their tractography algorithm. As lesions in the optic radiations were only observed in four patients and were reasonably small ($\leq$2 mm^3), the authors interpreted the displacement of the tracts and the alterations in connectivity values to indicate trans-synaptic degeneration. However, this was not confirmed by correlating the results with measures of optic nerve injury. More recently, Reich et al. [2009a] analyzed DTI from the optic radiations of 90 patients with MS and 29 healthy controls, to assess whether primary optic radiation injuries were associated with retinal injury and visual dysfunction. The authors performed a similar lengthwise analysis of the radiations to that described in this study, and this revealed significant increases in $\lambda_{||}$,

$\lambda_{\perp}$, and MD accompanied by a significant reduction in FA. Optic radiations $\lambda_{\perp}$, FA, and lesion volume were found to correlate with mean binocular RNFL thickness and low contrast letter acuity, suggesting that optic radiation injuries potentially lead to retrograde optic nerve degeneration and are relevant to visual dysfuntion. The finding that $\lambda_{||}$ was increased, rather than decreased as was observed in the current study, potentially reflects differences in disease duration, lesion load and progressive alterations in non-lesional white matter observed with increased MS duration. Specifically, patients recruited to the previous study were on average older (45 years, compared to 34 in this study) and had longer disease durations (8 years, compared to four). Importantly, the patients in the previous study had greater volume of inflammatory lesions in the radiations (5.9%, compared to 3.2%).

Several additional human imaging studies have revealed LGN and post-geniculate alterations in patients with optic nerve or retinal injury. Korsholm et al. [2007] demonstrated LGN atrophy and blood-oxygen level dependent changes in the LGN in optic neuritis patients in the months following presentation. Although measurements of LGN atrophy would have provided strong supporting evidence for our DTI results, we were unable to segment the LGN on T1 images due to difficulties identifying the boundaries of the nucleus.

Alterations in MTR in the visual cortices have also been reported in patients who presented with acute optic neuritis only 6 months previously [Audoin et al., 2006]. The authors hypothesized that, MTR being a marker for macromolecular density, cortical reductions in MTR might be associated with cortical neuronal changes such as degeneration, alterations to synaptic morphology, or neuroplasticity.

Two studies have demonstrated significant DTI alterations in the optic radiations of patients with early blindness [Shimony et al., 2006; Shu et al., 2009]. The former study demonstrated significant atrophy of the optic radiations in early blind patients as well as increased diffusivity and reduced anisotropy in visual pathway white matter [Shimony et al., 2006]. The latter study demonstrated a significant increase in $\lambda_{\perp}$ with an associated reduction in anisotropy, but no change in $\lambda_{||}$, in the optic radiations of early blind subjects, using a probability mapping method similar to that used in the current study [Shu et al., 2009]. The results of both these studies suggest that loss of visual input to LGN neurons can result in degeneration in the optic radiations although the precise alterations differ to those reported here.

In contrast, two diffusion imaging studies of patients with extant optic nerve injury [Inglese et al., 2001; Ueki et al., 2006], found no significant differences in diffusion measures between patients and controls in the optic radiations. However, both studies employed manual ROI definition rather than tractography for segmentation of the optic radiations, so it is possible that ROI misplacement could have reduced the sensitivity of the analyses.

Our finding of reduced $\lambda_{||}$ outside the context of acute axonal injury is novel and will require replication in future studies. Previous studies such as those of MacDonald et al. [2007a] in mice with traumatic brain injury or Concha et al. [2006] in human callosotomy patients have reported secondary increases in $\lambda_{||}$ post-acutely. However, those studies report DTI parameters from within the primary injury rather than in second order neuronal tracts. While, none of the aforementioned DTI studies in patients with optic nerve injury or early blindness reported reduced $\lambda_{||}$, differences in study cohorts and pathology could explain the discrepant results. For example, transsynaptic degeneration has been shown to be associated with neuronal atrophy rather than neuronal loss in MS [Evangelou et al., 2001] and we have previously shown that axonal atrophy is associated with reduced axial diffusivity in the optic nerves in a mouse model of MS [Wu et al., 2007]. Based on our results and these previous findings, we hypothesize that reduced $\lambda_{||}$ could be a DTI marker for anterograde trans-synaptic degeneration in the visual pathway.

Methodological Issues and Limitations

This study utilized a probabilistic atlas of the optic radiations calculated from control diffusion tractography data to obtain diffusivity and anisotropy measures from within the optic radiations specifically. We found that diffusivity and anisotropy measures calculated from two atlases produced from two independent subgroups of healthy subjects showed good agreement indicating that anatomical variation was minimal after nonlinear coregistration of FA maps. However, DTI parameters calculated using the atlas demonstrated poorer agreement with those obtained using subject specific tractography maps. Reich et al. [2009b] demonstrated that average DTI parameters calculated using a probability map exhibited lower coefficients of variation for repeated scanning of the same individual when compared to individual tractography results. Therefore, quantitative imaging results obtained from probability mapping techniques are potentially more reproducible than those obtained from traditional individual tractographic mapping.

The method for creating the probability map employed here differed in some ways to methods employed previously. In this study, tractography seed and target masks were defined in standard space using published brain atlases freely available with the FSL MRI analysis toolkit. The use of standard space masks can minimize the anatomical variability in ROI placement and enables greater flexibility in defining novel tracts of interest using various anatomical mask combinations. Excellent intersubject image coregistration is also imperative for probabilistic mapping, especially for clinical studies, where brain atrophy can displace white matter tracts. To minimise intersubject anatomical variability, we used a spatial normalization procedure, based on nonlinear alignment of the FA map to a standard space FA template image. The FA

image has high contrast in the centre of white matter tracts, such as the optic radiations. Therefore, image registrations based on the FA image will be biased toward more precise alignment of white matter tracts. Recently, DTI registration algorithms have been proposed which utilize the full 3D tensor to drive the registration process [Zhang et al., 2006]. Such registration schemes may improve inter-subject alignment and require further investigation in the context of clinical applications of DTI.

Limitations with the current study require brief discussion. First, the study was designed as a preliminary investigation to determine whether evidence existed for the presence of trans-synaptic degeneration in the primary visual pathway following optic neuritis. Although our results do support this hypothesis, a larger study of patients with acute optic neuritis, imaged prospectively after first presentation will be required to assess the timing of trans-synaptic degeneration following acute optic neuritis. In addition, the DWI sequences used to collect patient data altered during the study, unfortunately out of our control. In order to assess the potential effect of this change on our results, we acquired matching data from three control subjects and included "sequence" as a fixed factor in ANOVA. Although $\lambda_{\perp}$ and FA did display significant main effects for "sequence," no interactions were detected between "sequence" and "group," indicating that differences in $\lambda_{\perp}$ and FA related to DWI sequence did not influence group differences between people with optic neuritis and healthy control subjects. Importantly, we did not see a significant effect of "sequence" on the $\lambda_{||}$ or α values, which were found to correlate with optic nerve dysfunction.

CONCLUSIONS

This study provides preliminary evidence that optic nerve axonal degeneration following optic neuritis is associated with optic radiation injury, characterized by increased deviation and reduced magnitude of the principal direction of diffusion. A likely mechanism underlying this relationship is anterograde trans-synaptic degeneration, although such an interpretation requires replication in a larger prospective study. Given that progressive brain atrophy and neurological symptoms characteristic of secondary progressive MS cannot be explained by concurrent inflammatory activity, the pathological mechanisms of neurodegeneration are to be elucidated incontrovertibly. However, processes such as chronic trans-synaptic degeneration could be responsible, and diffusion tensor imaging could have a role in characterizing such secondary neurodegeneration in vivo.

ACKNOWLEDGMENTS

The authors thank all the participants in the study, Dr. Michael Ditchfield and Michael Kean at the Murdoch Children's Research Institute for MRI facility, Dr. Leonid Churilov from the Florey Neuroscience Institutes for advice regarding statistical analyses, and Dr. Alexander Klistorner and the Sydney Eye Hospital for invaluable advice and use of software for multifocal VEP analysis.

REFERENCES

Alexander D, Pierpaoli C, Basser P, Gee J (2001): Spatial transformations of diffusion tensor magnetic resonance images. IEEE Trans Med Imaging 20:1131–1139.

Altman DG, Bland J (1983): Measurement in medicine: The analysis of method comparison studies. Statistician 32:307–317.

Audoin B, Fernando KT, Swanton JK, Thompson AJ, Plant GT, Miller DH. (2006): Selective magnetization transfer ratio decrease in the visual cortex following optic neuritis. Brain 129 (Part 4):1031–1039.

Basser P, Mattiello J, LeBihan D (1994): Estimation of the effective self-diffusion tensor from the NMR spin echo. J Magn Reson B 103:247–254.

Behrens TE, Berg HJ, Jbabdi S, Rushworth MF, Woolrich MW (2007): Probabilistic diffusion tractography with multiple fibre orientations: What can we gain? Neuroimage 34:144–155.

Brex PA, Ciccarelli O, O'Riordan JI, Sailer M, Thompson AJ, Miller DH (2002): A longitudinal study of abnormalities on MRI and disability from multiple sclerosis. N Engl J Med 346:158–164.

Chard DT, Brex PA, Ciccarelli O, Griffin CM, Parker GJ, Dalton C, Altmann DR, Thompson AJ, Miller DH (2003): The longitudinal relation between brain lesion load and atrophy in multiple sclerosis: A 14 year follow up study. J Neurol Neurosurg Psychiatry 74:1551–1554.

Ciccarelli O, Toosy AT, Hickman SJ, Parker GJ, Wheeler-Kingshott CA, Miller DH, Thompson AJ (2005): Optic radiation changes after optic neuritis detected by tractography-based group mapping. Hum Brain Mapp 25:308–316.

Concha L, Gross DW, Wheatley BM, Beaulieu C (2006): Diffusion tensor imaging of time-dependent axonal and myelin degradation after corpus callosotomy in epilepsy patients. Neuroimage 32:1090–1099.

Costello F, Coupland S, Hodge W, Lorello GR, Koroluk J, Pan YI, Freedman MS, Zackon DH, Kardon RH (2006): Quantifying axonal loss after optic neuritis with optical coherence tomography. Ann Neurol 59:963–969.

Craner MJ, Newcombe J, Black JA, Hartle C, Cuzner ML, Waxman SG (2004): Molecular changes in neurons in multiple sclerosis: Altered axonal expression of Nav1.2 and Nav1.6 sodium channels and Na/Ca2 exchanger. Proc Natl Acad Sci USA 101:8168–8173.

DeBoy CA, Zhang J, Dike S, Shats I, Jones M, Reich DS, Mori S, Nguyen T, Rothstein B, Miller RH, et al. (2007): High resolution diffusion tensor imaging of axonal damage in focal inflammatory and demyelinating lesions in rat spinal cord. Brain 130 (Part 8):2199–2210.

Eickhoff SB, Stephan KE, Mohlberg H, Grefkes C, Fink GR, Amunts K, Zilles K (2005): A new SPM toolbox for combining probabilistic cytoarchitectonic maps and functional imaging data. NeuroImage 25:1325–1335.

Evangelou N, Konz D, Esiri MM, Smith S, Palace J, Matthews PM. (2001): Size-selective neuronal changes in the anterior optic pathways suggest a differential susceptibility to injury in multiple sclerosis. Brain 124 (Part 9):1813–1820.

Geurts JJ, Pouwels PJ, Uitdehaag BM, Polman CH, Barkhof F, Castelijns JA (2005): Intracortical lesions in multiple sclerosis: Improved detection with 3D double inversion-recovery MR imaging. Radiology 236:254–260.

Ghetti B, Horoupian DS, Wisniewski HM (1972): Transsynaptic response of the lateral geniculate nucleus and the pattern of degeneration of the nerve terminals in the rhesus monkey after eye enucleation. Brain Res 45:31–48.

Ginsberg SD, Martin LJ (2002): Axonal transection in adult rat brain induces transsynaptic apoptosis and persistent atrophy of target neurons. J Neurotrauma 19:99–109.

Glees P, Hasan M, Tischner K (1967): Ultrastructural features of transneuronal atrophy in monkey geniculate neurones. Acta Neuropathol 7:361–366.

Hua K, Zhang J, Wakana S, Jiang H, Li X, Reich DS, Calabresi PA, Pekar JJ, van Zijl PC, Mori S (2008): Tract probability maps in stereotaxic spaces: Analyses of white matter anatomy and tract-specific quantification. Neuroimage 39:336–347.

Inglese M, Rovaris M, Bianchi S, Comi G, Filippi M (2001): Magnetization transfer and diffusion tensor MR imaging of the optic radiations and calcarine cortex from patients with Leber's hereditary optic neuropathy. J Neurol Sci 188:33–36.

Jenkinson M, Smith S (2001): A global optimisation method for robust affine registration of brain images. Med Image Anal 5:143–156.

Johnson H, Cowey A (2000): Transneuronal retrograde degeneration of retinal ganglion cells following restricted lesions of striate cortex in the monkey. Exp Brain Res 132:269–275.

Jones D, Horsfield M, Simmons A (1999): Optimal strategies for measuring diffusion in anisotropic systems by magnetic resonance imaging. Magn Reson Med 42:515–525.

Klistorner A, Graham S, Fraser C, Garrick R, Nguyen T, Paine M, O'Day J, Grigg J, Arvind H, Billson F (2007): Electrophysiological evidence for heterogeneity of lesions in optic neuritis. Invest Ophthalmol Vis Sci 48:4549–4556.

Klistorner A, Arvind H, Nguyen T, Garrick R, Paine M, Graham S, O'Day J, Grigg J, Billson F, Yiannikas C (2008a) Inflammation, demyelination, and axonal loss in postacute optic neuritis. Ann Neurol 64:325–331.

Klistorner A, Arvind H, Nguyen T, Garrick R, Paine M, Graham S, O'Day J, Grigg JR, Billson FA, Yiannikas C (2008b) Inflammation, demyelination, and axonal loss in postacute optic neuritis. Ann Neurol 64:325–331.

Kolbe S, Chapman C, Nguyen T, Bajraszewski C, Johnston L, Kean M, Mitchell P, Paine M, Butzkueven H, Kilpatrick T, Egan G. (2009): Optic nerve diffusion changes and atrophy jointly predict visual dysfunction after optic neuritis. Neuroimage 45:679–686.

Korsholm K, Madsen KH, Frederiksen JL, Skimminge A, Lund TE (2007): Recovery from optic neuritis: An ROI-based analysis of LGN and visual cortical areas. Brain 130 (Part 5):1244–1253.

LeVay S (1971): On the neurons and synapse of the lateral geniculate nucleus of the monkey, and the effects of eye enucleation. Cell Tissue Res 113:396–419.

Lin F, Yu C, Jiang T, Li K, Chan P (2007): Diffusion tensor tractography-based group mapping of the pyramidal tract in relapsing-remitting multiple sclerosis patients. AJNR Am J Neuroradiol 28:278–282.

Mac Donald C, Dikranian K, Bayly P, Holtzman D, Brody D (2007a) Diffusion tensor imaging reliably detects experimental traumatic axonal injury and indicates approximate time of injury. J Neurosci 27:11869–11876.

Mac Donald CL, Dikranian K, Song SK, Bayly PV, Holtzman DM, Brody DL (2007b) Detection of traumatic axonal injury with diffusion tensor imaging in a mouse model of traumatic brain injury. Exp Neurol 205:116–131.

McDonald WI, Compston A, Edan G, Goodkin D, Hartung HP, Lublin FD, McFarland HF, Paty DW, Polman CH, Reingold SC, et al. (2001): Recommended diagnostic criteria for multiple sclerosis: Guidelines from the International Panel on the diagnosis of multiple sclerosis. Ann Neurol 50:121–127.

Mori S, Oishi K, Jiang H, Jiang L, Li X, Akhter K, Hua K, Faria AV, Mahmood A, Woods R, et al. (2008): Stereotaxic white matter atlas based on diffusion tensor imaging in an ICBM template. Neuroimage 40:570–582.

Naismith R, Xu J, Tutlam N, Snyder A, Benzinger T, Shimony J, Shepherd J, Trinkaus K, Cross A, Song S (2009): Disability in optic neuritis correlates with diffusion tensor-derived directional diffusivities. Neurology 72:589–594.

Pagani E, Filippi M, Rocca MA, Horsfield MA (2005): A method for obtaining tract-specific diffusion tensor MRI measurements in the presence of disease: Application to patients with clinically isolated syndromes suggestive of multiple sclerosis. Neuroimage 26:258–265.

Peltier J, Travers N, Destrieux C, Velut S (2006): Optic radiations: A microsurgical anatomical study. J Neurosurg 105:294–300.

Reich D, Smith S, Gordon-Lipkin E, Ozturk A, Caffo B, Balcer L, Calabresi P (2009a) Damage to the optic radiaion in multiple sclerosis is associated with retinal injury and visual disability. Arch Neurol 66:1–10.

Reich DS, Ozturk A, Calabresi PA, Mori S (2009b) Automated vs. conventional tractography in multiple sclerosis: Variability and correlation with disability. Neuroimage 49:3047–3056.

Reich DS, Smith SA, Gordon-Lipkin EM, Ozturk A, Caffo BS, Balcer LJ, Calabresi PA. (2009c) Damage to the optic radiaion in multiple sclerosis is associated with retinal injury and visual disability. Arch Neurol 66:1–10.

Rorden C, Brett M (2000): Stereotaxic display of brain lesions. Behav Neurol 12:191–200.

Rovaris M, Filippi M (2007): Diffusion tensor MRI in multiple sclerosis. J Neuroimaging 17 (Suppl 1):27S–30S.

Rovaris M, Gass A, Bammer R, Hickman SJ, Ciccarelli O, Miller DH, Filippi M (2005): Diffusion MRI in multiple sclerosis. Neurology 65:1526–1532.

Shimony JS, Burton H, Epstein AA, McLaren DG, Sun SW, Snyder AZ (2006): Diffusion tensor imaging reveals white matter reorganization in early blind humans. Cereb Cortex 16:1653–1661.

Shu N, Li J, Li K, Yu C, Jiang T (2009): Abnormal diffusion of cerebral white matter in early blindness. Hum Brain Mapp 30:220–227.

Smith SM, Jenkinson M, Woolrich MW, Beckmann CF, Behrens TE, Johansen-Berg H, Bannister PR, De Luca M, Drobnjak I, Flitney DE, et al. (2004): Advances in functional and structural MR image analysis and implementation as FSL. Neuroimage 23 (Suppl 1):S208–S219.

Song SK, Sun SW, Ju WK, Lin SJ, Cross AH, Neufeld AH (2003): Diffusion tensor imaging detects and differentiates axon and myelin degeneration in mouse optic nerve after retinal ischemia. Neuroimage 20:1714–1722.

Song SK, Yoshino J, Le TQ, Lin SJ, Sun SW, Cross AH, Armstrong RC (2005): Demyelination increases radial diffusivity in corpus callosum of mouse brain. Neuroimage 26:132–140.

Trapp BD, Peterson J, Ransohoff RM, Rudick R, Mork S, Bo L (1998): Axonal transection in the lesions of multiple sclerosis. N Engl J Med 338:278–285.

Trip S, Wheeler-Kingshott C, Jones S, Li W, Barker G, Thompson A, Plant G, Miller D (2006a) Optic nerve diffusion tensor imaging in optic neuritis. NeuroImage 30:498–505.

Trip SA, Schlottmann PG, Jones SJ, Li WY, Garway-Heath DF, Thompson AJ, Plant GT, Miller DH (2006b) Optic nerve atrophy and retinal nerve fibre layer thinning following optic neuritis: Evidence that axonal loss is a substrate of MRI-detected atrophy. Neuroimage 31:286–293.

Ueki S, Fujii Y, Matsuzawa H, Takagi M, Abe H, Kwee IL, Nakada T (2006): Assessment of axonal degeneration along the human visual pathway using diffusion trace analysis. Am J Ophthalmol 142:591–596.

van Buren JM (1963): Trans-synaptic retrograde degeneration in the visual system of primates. J Neurol Neurosurg Psychiatry 26:402–409.

Wheeler-Kingshott CA, Cercignani M (2009): About "axial" and "radial" diffusivities. Magn Reson Med 61:1255–1260.

Wu Q, Butzkueven H, Gresle M, Kirchhoff F, Friedhuber A, Yang Q, Wang H, Fang K, Lei H, Egan GF, et al. (2007): MR diffusion changes correlate with ultra-structurally defined axonal degeneration in murine optic nerve. Neuroimage 37:1138–1147.

Wu QZ, Yang Q, Cate HS, Kemper D, Binder M, Wang HX, Fang K, Quick MJ, Marriott M, Kilpatrick TJ, et al. (2008): MRI identification of the rostral-caudal pattern of pathology within the corpus callosum in the cuprizone mouse model. J Magn Reson Imaging 27:446–453.

Xie S, Gong GL, Xiao JX, Ye JT, Liu HH, Gan XL, Jiang ZT, Jiang XX (2007): Underdevelopment of optic radiation in children with amblyopia: A tractography study. Am J Ophthalmol 143:642–646.

Zhang H, Yushkevich PA, Alexander DC, Gee JC (2006): Deformable registration of diffusion tensor MR images with explicit orientation optimization. Med Image Anal 10:764–785.

Zhang J, Jones M, DeBoy CA, Reich DS, Farrell JA, Hoffman PN, Griffin JW, Sheikh KA, Miller MI, Mori S, et al. (2009): Diffusion tensor magnetic resonance imaging of Wallerian degeneration in rat spinal cord after dorsal root axotomy. J Neurosci 29:3160–3171.